Correct Boundary Conditions for the High-Resolution Model of Nonlinear Acoustic-Gravity Waves Forced by Atmospheric Pressure Variations

4 authors, including:

Sergey Kshevetskii
Immanuel Kant Baltic Federal University
88 PUBLICATIONS   **249** CITATIONS

SEE PROFILE

Nikolai M. Gavrilov
Saint Petersburg State University
253 PUBLICATIONS   **1,235** CITATIONS

SEE PROFILE

S. N. Kulichkov
Obukhov Institute of Atmospheric. Physics RAS
92 PUBLICATIONS   **494** CITATIONS

SEE PROFILE

Some of the authors of this publication are also working on these related projects:

Climate Physics Theory View project

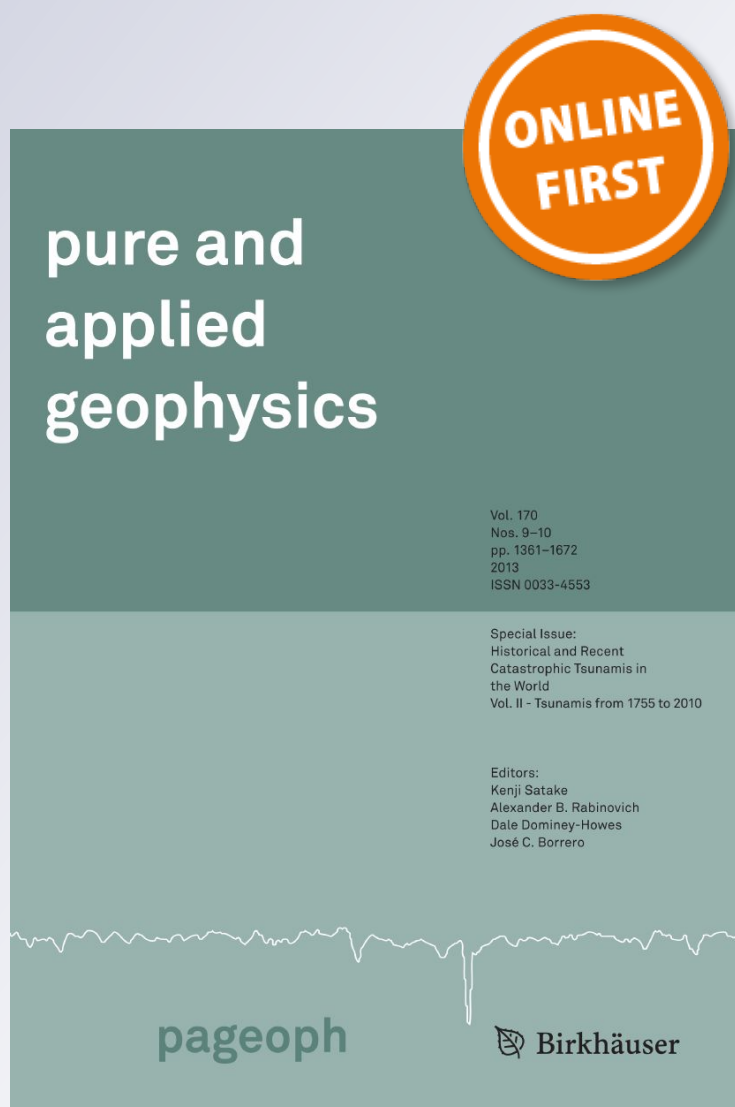Wave-mean flow nonlinear interactions in the middle atmosphere View project

Correct Boundary Conditions for the High-Resolution Model of Nonlinear Acoustic-Gravity Waves Forced by Atmospheric Pressure Variations

Yu. A. Kurdyaeva, S. P. Kshevetskii, N. M. Gavrilov & S. N. Kulichkov

pure and
applied
geophysics

Vol. 170
Nos. 9–10
pp. 1361–1672
2013
ISSN 0033-4553

Special Issue:
Historical and Recent
Catastrophic Tsunamis in
the World
Vol. II - Tsunamis from 1755 to 2010

Editors:
Kenji Satake
Alexander B. Rabinovich
Dale Dominey-Howes
José C. Borrero

pageoph   ⚡ Birkhäuser

⌬ Springer

Springer

Pure and Applied Geophysics

CrossMark

Correct Boundary Conditions for the High-Resolution Model of Nonlinear Acoustic-Gravity Waves Forced by Atmospheric Pressure Variations

Yu. A. Kurdyaeva,[1] · S. P. Kshevetskii,[1] N. M. Gavrilov,[2] and S. N. Kulichkov[3]

Abstract—Currently, an international network of operating high-resolution microbarographs was established to record wave-induced pressure variations at the Earth's surface. Based on these measurements, simulations are performed to analyze the characteristics of waves corresponding to the observed variations of atmospheric pressure. Such a mathematical problem involves a set of primitive nonlinear hydrodynamic equations considering lower boundary conditions in the form of pressure variations at the Earth's surface. Selection of upward propagating acoustic-gravity waves (AGWs) generated or reflected at the Earth's surface requires the Neumann boundary conditions involving the vertical gradients of vertical velocity at the lower boundary. To analyze the correctness of the mathematical problem, linearized equations are used for small-surface wave amplitudes excited near the ground. Using the relation for wave energy, it is proven that the solution of the boundary problem based on the nondissipative approximation is uniquely determined by the variable pressure field at the Earth's surface. The respective dissipative problem has also a unique solution with the appropriate choice of lower boundary conditions for temperature and velocity components. To test the numerical algorithm, solutions of the linearized equations for AGW modes are used. Developed boundary conditions are implemented into the model describing acoustic-gravity wave propagation from the surface atmospheric pressure source. Atmospheric waves propagating from the observed surface pressure variations to the upper atmosphere are simulated using the obtained algorithms and the computer codes.

[1] Institute of Physical-Mathematical Sciences and Information Technologies, Baltic Federal University, Kaliningrad, Russia. E-mail: spkshev@gmail.com
[2] Atmospheric Physics Department, Saint Petersburg State University, St. Petersburg, Russia.
[3] Obukhov Institute of Atmospheric Physics, Russian Academy of Science, Moscow, Russia.

Birkhäuser

1. Introduction

Acoustic-gravity waves (AGWs) are observed in the atmosphere almost permanently. According to recent knowledge, atmospheric AGWs propagating in the middle and upper atmosphere can be excited within the troposphere. These waves can be generated by mesoscale turbulence and convection (Fritts and Alexander 2003; Fritts et al. 2006), atmospheric fronts and jet streams (e.g., Gavrilov and Fukao 1999; Plougonven and Snyder 2007; Plougonven and Zhang 2014) with maximum wave excitation efficiency at altitudes 9–12 km (e.g., Medvedev and Gavrilov 1995; Dalin et al. 2016). Generated waves can propagate from the troposphere to the middle and upper atmosphere, where they can break and produce instabilities and turbulence (e.g., Fritts and Alexander 2003; Gavrilov and Yudin 1992; Gavrilov and Fukao 1999). AGW appearance is often associated with meteorological phenomena (Blanc et al. 2014). The formation and evolution of cumulus clouds, water phase transitions, and respective heating/cooling mainly lead to the generation of AGWs affecting the processes in the atmosphere (e.g., Pierce and Coroniti 1966; Balachandran 1980; Fovell et al. 1992a, b; Miller 1999; Alexander et al. 2004; Blanc et al. 2014). The works by Pedloski (2006), Brekhovskikh and Godin (1990) and Leble and Perelomova (2013) are devoted to an analytical study of the AGW propagation in the atmosphere.

To simulate atmospheric AGWs and turbulence, numerical models based on nonlinear primitive hydrodynamic equations are recently used. Baker and Schubert (2000) simulated propagation of nonlinear waves in the atmosphere of Venus in a localized area with a horizontal and vertical dimension of 120 and

48 km, respectively. Fritts and Garten (1996) and Andreassen et al. (1998) simulated Kelvin–Helmholtz instabilities and turbulence generation by breaking internal gravity waves. They used atmospheric areas with a relatively small vertical and horizontal dimension, and applied Halerkin-type algorithms, based on the conversion of initial hydrodynamic equations into sets of equations for spectral components. Yu et al. (2009) and Liu et al. (2008) developed two-dimensional numerical models for propagating atmospheric AGWs.

Frequently, high-resolution models are used for simulations of meso- and macroscale processes, especially for forecasts of meteorological phenomena and weather prediction (global circulation models are not considered). Among such models, one can mention the well-known WRF-NMM or NAM model (Janjic 2002, 2006) from the WRF series, as well as the RAMS model (Pielke et al. 1992) and other models, like DNS models (Babkovskaia et al. 2011) and LES models (Khairoutdinov et al. 2009). These models were developed to simulate atmospheric processes, regionally and in smaller scales. The models are based on numerical solution of hydrodynamic equations and differ in numerical methods and parameterizations, or by the absence of parameterizations, as the DNS. Additionally, the models differ in scales, modeling of humidity, etc.

Simulations of AGWs from meteorological sources (Kshevetskii and Kulichkov 2015; Jonson and Young 1983; Sao Sabbas et al. 2009) revealed big variation in the parameters of heat wave sources in the atmosphere. The available meteorological data are often insufficient for a detailed description of convective thermal sources, which can generate atmospheric AGWs (Jonson and Young 1983; Sao Sabbas et al. 2009; Kshevetskii and Kulichkov 2015). Modeling waves from specific meteorological sources (Fovell et al. 1992a, b; Baker and Schubert 2000; Andreassen et al. 1998; Yu et al. 2009) gave the scales and frequencies of the simulated waves roughly corresponding to the observed waves; however, the amplitudes were quite different from the real ones due to the uncertainty in the wave source parameters. This requires more precise specification of AGW sources in the numerical models simulating atmospheric AGWs.

Gavrilov and Kshevetsky (2013, 2015) simulated AGWs propagating from the lower atmosphere and breaking at high altitudes. In the regions of wave breakdown, the smoothness of mathematical solution is often lost. Therefore, the fulfillment of the fundamental conservation laws (mass, momentum, and energy) in the numerical model is important. Lax (1957) and Lax and Wendroff (1960) have shown that when the fundamental conservation laws are precisely satisfied, the numerical method gives physically correct non-smooth solutions of the equations. This allows us to simulate AGW breaking, even in the case of non-smooth solutions. Gavrilov and Kshevetskii (2014a) extended their 2D model to a 3D version. They studied the thermal structure and the generation of jet streams in the upper atmosphere caused by dissipating AGWs which originated from a stationary source at the Earth's surface.

Kshevetskii and Kulichkov (2015) used the 3D nonlinear model for the description of the AGW generation by heating/cooling of atmospheric gas in water-phase transitions during evolutions of thunderstorm clouds. Particularly, they studied the relation between local pressure variations and the formation or rather the development of thunderclouds, and simulated AGW propagation to the middle and upper atmosphere. Karpov and Kshevetskii (2014) modeled AGW propagation from a local, non-stationary source located at the Earth's surface. They showed that infrasound waves (having periods of 2–3 min or less) originating in the troposphere could create jet streams and significantly (up to 10 K and more) warm up the upper atmosphere. These effects require further detailed studies because of great diversity of their characteristics.

Processes of cumulus cloud evolution lead to AGW generation (e.g., Blanc et al. 2014; Alexander et al. 2004). These waves can propagate downwards and can be reflected at the rigid Earth's surface back to the atmosphere. They can cause fluctuations of the surface pressure (Blanc et al. 2014; Kshevetskii and Kulichkov 2015), which are recorded at the networks of high-sensitive microbarographs existing and actively expanding, for example, in Europe and Africa (Blanc et al. 2014). Surface pressure variations contain information about waves generated and/or reflected at the ground and can be used as the lower

boundary in the numerical simulations of AGWs propagating from the Earth's surface to the atmosphere.

Using the surface pressure as the lower boundary conditions in nonlinear numerical AGW models raise some difficulties. Usually, microbarograph pressure measurements do not provide other wave fields with the same resolution and accuracy for the assimilation into the model. In addition, the lower boundary of the model should incorporate AGWs being generated or reflected at the Earth's surface and propagating upwards to the atmosphere. From mathematical point of view, such waves are equivalent to AGWs with positive vertical wave flux pw > 0. Additionally, such waves should follow relations of traditional AGW theory (e.g., Gossard and Hook 1975) above turbulized dissipative boundary layer.

Our analysis showed that Dirichlet boundary conditions of the first kind (e.g., Courant and Hilbert 1962), containing the values of hydrodynamic fields, could not select upward propagating AGWs. For example, the frequently used condition $w = 0$ for wave sources located inside the atmosphere gives the energy flux pw = 0 at the lower boundary. Therefore, only reflected waves can propagate upwards near the lower boundary.

Handling polarization relations of traditional AGW theory as the lower boundary conditions for unmeasured wave fields does not give satisfactory results due to dependency of these relations on AGW frequency and wavelength, which are not measured and can highly vary during the simulations. In addition, high turbulent viscosity and heat conduction in the boundary layer can violate polarization relations of nondissipative AGW theory (e.g., Gavrilov and Kshevetskii 2015).

In this paper, we show that the upward propagating AGWs generated and reflected at the ground and corresponding to microbarograph pressure variations can be effectively selected with the Neumann boundary conditions of the "second kind", which involves vertical gradients of wave hydrodynamic fields (e.g., Courant and Hilbert 1962). For simulations, we used the high-resolution three-dimensional numerical model of nonlinear AGWs developed and described by Gavrilov and Kshevetsky (2014a, b) and Gavrilov and Kshevetskii (2015), which is now freely

available online (AtmoSym 2016). This study should provide a new manner of AGW excitation at the lower boundary of the model, based on observations.

Meteorological models take into account some part of the AGW spectrum, but these models normally ignore AGWs with periods less than a few minutes; these ignored short-period waves can propagate from the lower atmosphere to the upper atmosphere and they are very interesting for the upper atmosphere physics. In addition, between the Earth's surface and an altitude of about 500 km, the atmospheric density decreases by 13 orders of magnitude, which imposes special demands to the calculation methods implemented in the AtmoSym.

In Sect. 2, we perform a mathematical analysis on a set of primitive hydrodynamic equations and boundary conditions used in the AtmoSym model. Section 3 considers the correct formulation of the Neumann boundary condition (second kind) including vertical gradients of the vertical velocity. In this way, vertically upward propagating AGWs are initialized which are generated or reflected at the Earth's surface. Nonlinear equations are difficult for strict mathematical analysis. However, wave amplitudes at the Earth's surface are usually small so that the study can also be based on linearized equations.

In Sect. 4, we describe the comparison of numerically simulated AGWs with analytical solution to the linearized nondissipative equations near the ground. The comparison shows that discrepancies between numerical solution and linear model exists only inside the thin (several meters) turbulized and dissipative boundary layer. In the free atmosphere, the numerical solution/approach for the second-kind lower boundary conditions fits reasonably well to the analytical solution of the linear AGW theory. Section 5 is dedicated to the model experiment of AGWs propagating from a localized region based on the microbarograph observations.

2. Numerical Model

In the present paper, we mainly consider the three-dimensional high-resolution numerical model AtmoSym simulating atmospheric AGWs, which was developed by Gavrilov and Kshevetskii (2014a, b)

and Gavrilov and Kshevetskii (2015). Recently, this supercomputer mathematical model is freely online available (see AtmoSym 2016). The AtmoSym supercomputer model can simulate propagation of nonlinear AGWs from various initial disturbances and wave sources in an altitude range between 0 and 500 km. The model is equipped with a convenient push-button control system. The model takes into account the Coriolis force in the *f*-plane approximation, but it can be also disabled if its effect is negligible.

The model with the appropriate selection of the control parameters maybe used as a DNS system, especially in the upper atmosphere, where the mean free path is larger than the model grid spacing. However, a possible account of turbulent viscosity is also provided in the model, and it is advisable at lower altitudes if large grid steps are applied and if the simulation time is long. The model can also be used to simulate the propagation of AGW from an oscillating surface.

The AtmoSym model has been developed for studies of the upper atmosphere dynamic. Historically, he upper atmosphere models were developed independently of meteorological models for a long time. Gradually it was found out that some processes in the lower atmosphere affect the processes in the upper atmosphere. Thus, the troposphere and lower stratosphere were included as lower boundary of AtmoSym and other upper atmosphere models.

The computer 3D AtmoSym model allows solving the problems of wave propagation from various initial disturbances and wave sources in the atmospheric region with the vertical extension of 0–500 km and the horizontal extension of several 1000 km. A user of the model can regulate the grid resolution depending on the problem being solved and on the power of the supercomputer used. The optimal grid size in the vertical plane is a non-uniform one and is constructed by the model automatically, taking into account the atmosphere stratification. Near the Earth's surface, the vertical grid is eight times smaller than in 500 km. In the default version, the average vertical grid spacing is 250 m, and the grid size near the Earth's surface is less than 100 m. The grid resolution in the horizontal plane can be adjusted and usually it lies in the range of 250 m–4 km. The model provides also the possibility of using a non-uniform horizontal grid specified by users. The required time step is depending on the condition of stability and convergence of the method. The time step varies between 0.1 s and a few seconds for the horizontal grid step between 0.25 and 4 km, respectively. The AtmoSym uses three levels of parallel computations. The distribution of computing on cluster nodes is provided with Message Passing Interface (MPI). On each cluster node, the computations are parallelized using Open Multi-Processing (OpenMP); parallelization of computations in processor's cores is established automatically, using SSEx.

2.1. Nonlinear Hydrodynamic Equations

The AtmoSym numerical model solves a set of primitive hydrodynamic equations using the continuity equation (Eq. 1), the motion equations (Eq. 2), the internal energy equation rewritten as the pressure equation under the assumption of the ideal gas state (Eq. 3), and the ideal gas state equation (Eq. 4):

$$\frac{\partial \rho}{\partial t} + \frac{\partial \rho u}{\partial x} + \frac{\partial \rho v}{\partial y} + \frac{\partial \rho w}{\partial z} = 0, \tag{1}$$

$$\frac{\partial \rho u}{\partial t} + \frac{\partial \rho u^2}{\partial x} + \frac{\partial \rho uv}{\partial y} + \frac{\partial \rho uw}{\partial z} + 2\rho \omega_z v$$
$$= -\frac{\partial p}{\partial x} + \left(\frac{\partial^2}{\partial x^2} + \frac{\partial^2}{\partial y^2}\right)\varsigma(z)u + \frac{\partial}{\partial z}\varsigma(z)\frac{\partial u}{\partial z},$$

$$\frac{\partial \rho v}{\partial t} + \frac{\partial \rho uv}{\partial x} + \frac{\partial \rho v^2}{\partial y} + \frac{\partial \rho vw}{\partial z} - 2\rho \omega_z u$$
$$= -\frac{\partial p}{\partial y} + \left(\frac{\partial^2}{\partial x^2} + \frac{\partial^2}{\partial y^2}\right)\varsigma(z)v + \frac{\partial}{\partial z}\varsigma(z)\frac{\partial v}{\partial z}, \tag{2}$$

$$\frac{\partial \rho w}{\partial t} + \frac{\partial \rho uw}{\partial x} + \frac{\partial \rho vw}{\partial y} + \frac{\partial \rho w^2}{\partial z}$$
$$= -\frac{\partial p}{\partial z} - \rho g + \left(\frac{\partial^2}{\partial x^2} + \frac{\partial^2}{\partial y^2}\right)\varsigma(z)w + \frac{\partial}{\partial z}\varsigma(z)\frac{\partial w}{\partial z},$$

$$\frac{1}{\gamma-1}\left(\frac{\partial p}{\partial t} + \frac{\partial pu}{\partial x} + \frac{\partial pv}{\partial y} + \frac{\partial pw}{\partial z}\right) = -p\left(\frac{\partial u}{\partial x} + \frac{\partial v}{\partial y} + \frac{\partial w}{\partial z}\right)$$

$$+ \left(\frac{\partial^2}{\partial x^2} + \frac{\partial^2}{\partial y^2}\right)\kappa(z)T + \frac{\partial}{\partial z}\kappa(z)\frac{\partial(T')}{\partial z}$$

$$+ Q_{\text{visc}}, \quad Q_{\text{visc}} = \varsigma(z)\left[\left(\frac{\partial u}{\partial x}\right)^2 + \left(\frac{\partial u}{\partial y}\right)^2 + \left(\frac{\partial u}{\partial z}\right)^2\right.$$

$$+ \left(\frac{\partial v}{\partial x}\right)^2 + \left(\frac{\partial v}{\partial y}\right)^2 + \left(\frac{\partial v}{\partial z}\right)^2 + \left(\frac{\partial w}{\partial x}\right)^2$$

$$\left. + \left(\frac{\partial w}{\partial y}\right)^2 + \left(\frac{\partial w}{\partial z}\right)^2\right]. \tag{3}$$

$$p = \rho R_{\text{g}} T/\mu \tag{4}$$

In Eqs. (1)–(4), t is time; x, y, z and u, v, w are coordinates and velocity components directed, respectively, eastwards, northwards, and upwards; p, ρ, T are pressure, density, and temperature; R_{g} is the universal gas constant; μ is the air molecular weight; g is the acceleration of gravity; γ is the heat capacity ratio; ς and κ are the dynamic viscosity and thermal conductivity.

Equations (1)–(4) take into account nonlinear and dissipative processes accompanying wave propagation. They can describe, in particular, such complex phenomena as the formation of shock waves, the wave breaking and turbulence generation. The
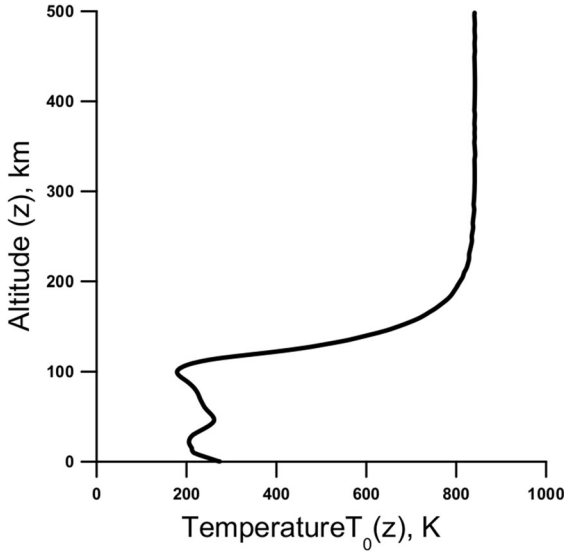

Figure 1
Vertical profile of the background temperature T_0 (z) from the semi-empirical atmospheric model NRL-MSISE-00 (Picone et al. 2002)

AtmoSym numerical model provides a self-consistent description of wave processes and takes into account the changes in atmospheric parameters due to energy transfer from dissipating waves to the atmosphere.

The vertical profiles of the background temperature $T_0(z)$ are taken from the semi-empirical atmospheric model NRL-MSISE-00 (Picone et al. 2002) from the Earth's surface up to 500 km, depending on solar activity indexes, day of year, local time, and geographical coordinates. Used $T_0(z)$ is shown in Fig. 1. Molecular kinematic viscosity is calculated using the formula of Banks and Kokarts (1973):

$$v(z) = \zeta(z)/\rho_0(z) = 3.4 \times 10^{-7} T_0(z)/\rho_0(z). \tag{5}$$

The molecular thermal conductivity coefficient is obtained by dividing the coefficient of viscosity by the Prandtl number. Similar expressions for molecular viscosity and thermal conductivity were used by Yu et al. (2009) and Liu et al. (2010). The AtmoSym model also takes into account vertical profiles of the background turbulent viscosity and thermal conductivity with a maximum about 10 m^2 s^{-1} near the ground and at an altitude of 100 km, and a minimum of 0.1 m^2 s^{-1} in the stratosphere (see Gavrilov 2013). The model does not consider effects like the dissipation due to ion drag or radiative heat exchange which are less important for high-frequency AGW.

2.2. Boundary Conditions

The AtmoSym model simulates waves in a limited atmospheric region. For analyzing spectral AGW components, periodical conditions at horizontal boundaries are frequently appropriate. Let L_x and L_y be the dimensions of the model area along axes x and y, respectively, therefore, the periodical horizontal boundary conditions have the following form:

$$
\begin{aligned}
u(x=L_x,y,z,t) &= u(x=0,y,z,t), & u(x,y=L_y,z,t) &= u(x,y=0,z,t), \\
v(x=L_x,y,z,t) &= v(x=0,y,z,t), & v(x,y=L_y,z,t) &= v(x,y=0,z,t), \\
w(x=L_x,y,z,t) &= w(x=0,y,z,t), & w(x,y=L_y,z,t) &= w(x,y=0,z,t), \\
p(x=L_x,y,z,t) &= p(x=0,y,z,t), & p(x,y=L_y,z,t) &= p(x,y=0,z,t), \\
\rho(x=L_x,y,z,t) &= \rho(x=0,y,z,t), & \rho(x,y=L_y,z,t) &= \rho(x,y=0,z,t), \\
T(x=L_x,y,z,t) &= T(x=0,y,z,t), & T(x,y=L_y,z,t) &= T(x,y=0,z,t).
\end{aligned}
\tag{6}
$$

At the top of the model, standard upper boundary conditions for wave propagation in thermosphere are used:

$$\frac{\partial T}{\partial z}\big|_{z=h}=0,\ \frac{\partial u}{\partial z}\big|_{z=h}=0,\ \frac{\partial v}{\partial z}\big|_{z=h}=0,\ w|_{z=h}=0. \tag{7}$$

The preferred reference height h is 500 km or more. These boundary conditions can create reflection of simulated waves at the upper boundary. Since the upper boundary conditions (7) are used for altitudes of 500 km or more, the reflected waves are dissipating due to high values of molecular viscosity and heat conduction. Sensitivity tests showed that the influence of the upper boundary conditions (7) is small at altitudes $z < h - 2H$; here H is taken for the altitudes $h \approx 500$ km and $H \approx 60$ km.

At the Earth's surface, the conditions for velocity components can be specified. Most frequently, the air non-flow through the surface is supposed, when w (x, y, $z = 0$, t) = 0. The vertical velocity component w (t, $z = 0$, x, y) is normally equal to zero, but for model experiments of earthquakes, tsunamis (Matsumura et al. 2011; Kherani et al. 2012; Shinagawa et al. 2007) or vertical vibrations of gas caused by convection (Fovell et al. 1992a, b; Snively and Pasko 2003), w (t, $z = 0$, x, y) is specified on the basis of experimental observations or assumptions of the considered phenomena. The condition of air adhesion is given by u (x, y, $z = 0$, t) = 0 and v (x, y, $z = 0$, t) = 0. In addition, the lower boundary conditions for the relative variation of the pressure, density, and temperature have to be specified

$$P = p'/p_0 = (p - p_0)/p_0,\ R = \rho'/\rho_0$$
$$= (\rho - \rho_0)/\rho_0,\ \Theta = T'/T_0 = (T - T_0)/T_0, \tag{8}$$

where the primes denote deviations of hydrodynamic fields from respective background values denoted with zero subscripts. In the present study, we use the surface pressure measurements as the lower boundary condition;

$$P(x, y, z = 0, t) = f_p(x, y, t), \tag{9}$$

where f_p (x, y, t) is an approximation function to the surface measurement data. The function f_p (x, y, t) has to be somehow appropriately constructed on the basis of discrete digitized pressure fluctuation records at fixed points where microbarographs are located. The boundary condition (9) was not used previously in atmospheric AGW simulations. It requires correct lower boundary conditions for the other hydrodynamic variables, which allows selecting upward AGWs propagating to the atmosphere. Therefore, the proper options for getting correct mathematical boundary problems are considered below.

3. Correctness of the Boundary Problem

System of nonlinear Eqs. (1)–(4) is complex and difficult for analysis. Near the Earth's surface, wave amplitudes are usually very small. Therefore, the equation is simplified by removing the nonlinear terms (see Gossard and Hooke 1975).

3.1. Correctness of Linearized Nondissipative Problem

The linearized equation set obtained from Eqs. (1) to (4) for the case of two spatial variables neglecting viscous and heat conduction terms can be represented in the following form (Kshevetskii 2001, 2002):

$$(\rho_0 R)_t + (\rho_0 u)_x + (\rho_0 w)_z = 0;\ P = R + \Theta,$$

$$(\rho_0 u)_t + (p_0 P)_x = 0;\ (\rho_0 w)_t + (p_0 P)_z + \rho_0 g R = 0, \tag{10}$$

$$(\rho_0 \Theta)_t - (\gamma - 1)(p_0 P)_t/c_s^2 + \rho_0 w N^2/g = 0,$$

where $N = \sqrt{\frac{(\gamma-1)}{\gamma}\frac{g}{H}}$ is the Brunt–Väisälä frequency; subscripts t, x, and z denote respective differentiation. Equation (10) is obtained for zero background wind, because the wind is usually small near the ground. The case of inclusion of viscosity and thermal conductivity is discussed in the next section. Two-dimensional equations are considered here for simplicity. The three-dimensional analysis is similar, but formulae are more bulky. In the two-dimensional case, the Coriolis forces are omitted. The initial conditions correspond to the lack of motions at $t = 0$:

$$u(x, z, t = 0) = 0,\ w(x, z, t = 0) = 0,\ R(x, z, t = 0)$$
$$= 0,\ \Theta(x, z, t = 0) = 0. \tag{11}$$

At horizontal boundaries, the two-dimensional version of periodical conditions (6) is used. The upper boundary condition

$$w(x, z = h, t) = 0, \qquad (12)$$

corresponds to Eq. (7). At the lower boundary we impose the condition (10), which can be rewritten as

$$P(x, z = 0, t) = [R(x, z = 0, t) + \Theta(x, z = 0, t)]$$
$$= f_p(x, t). \qquad (13)$$

The most important property of the correct solution is its uniqueness. In this respect, the following theorem can be formulated:

Theorem 1 *If a continuous solution of Eq.* (10) *with initial conditions* (11) *and boundary conditions* (6), (12) *and* (13) *exists, then it is unique.*

The proof of this theorem is given in the Online Appendix A. This theorem has a consequence.

Consequence Theorem 1 stated that in the nondissipative case the solution is only uniquely determined by the pressure variations (13) at the lower boundary, but not by the distributions and variations of density R and temperature Θ, also variations of horizontal velocity u. If an arbitrary function to R is added and subtracted from Θ, then the sum $R + \Theta = P$ on the boundary surface remains the same. Then the problem's solution does not change and remains the same.

However, arbitrary boundary conditions for u, R and Θ may lead to jumps in the hydrodynamic fields near the lower boundary $z = 0$ in linearized nondissipative model. In nonlinear models, such jumps can produce instabilities and generate mathematical wave modes that do not exist in the nature. Therefore, nonlinear models require specified self-consistent lower boundary conditions for u, R and Θ in addition to the condition (13) to minimize possible jumps and influence of mathematical wave modes.

3.2. Correctness of Linearized Dissipative Problem

In a linearized set of hydrodynamic equations for the case of two spatial dimensions, the dissipative terms are taken into account as follows:

$$(\rho_0 R)_t + (\rho_0 u)_x + (\rho_0 w)_z = 0; \ P = R + \Theta,$$

$$(\rho_0 u)_t + (p_0 P)_x = [\varsigma(z)u]_{xx} + [\varsigma(z)(w)_z]_z, \qquad (14)$$

$$(\rho_0 w)_t + (p_0 P)_z + \rho_0 gR = [\varsigma(z)w]_{xx} + [\varsigma(z)(w)_z]_z,$$

$$(\rho_0 \Theta)_t - (\gamma - 1)(p_0 P)_t/c_s^2 + \rho_0 wN^2/g$$
$$= (\gamma - 1)[(\kappa(z)T_0\Theta)_{xx} + (\kappa(z)(T_0\Theta)_z)_z]/c_s^2.$$

We apply the initial conditions (11) corresponding to the lack of motions at $t = 0$.

According to (7), the upper boundary has the form of

$$(T_0\Theta)_z|_{z=h} = 0, \ u_z|_{z=h} = 0, \ w(z = h) = 0. \qquad (15)$$

Analogous to Online Appendix A, the following uniqueness theorem can be proved:

Theorem 2 *If a continuous solution exits for the Eqs.* (14) *with initial conditions* (11) *and boundary conditions* (6), (13), (15) *and*

$$u|_{z=0} = 0, \quad w_z|_{z=0} = 0, \quad \Theta|_{z=0} = 0, \qquad (16)$$

then it is unique.

This theorem is proved in the Online Appendix B. The last boundary condition in (16) leads to the following lower boundary condition for density variations:

$$R(x, z = 0, t) = f_p(x, t) - \Theta(x, z = 0, t). \qquad (17)$$

This condition should be added to the lower boundary conditions (13) and (16) when the nonzero variations of pressure are specified at the Earth's boundary for studies of AGW propagation.

As far as AGW amplitudes are usually small near the ground, one should expect that the solutions of nonlinear and linearized equations are approximately equal near the lower boundary. Therefore, in the present study we solve the following nonlinear AGW boundary problem: (a) the equation set is (1)–(4); (b) zero initial conditions like (11); (c) the horizontal boundary conditions (6); (d) the lower boundary conditions (9), (16) and (17).

4. Comparisons of Nonlinear and Linearized Models

To study the influence of the lower boundary condition, we made comparisons of simulations using the nonlinear Eqs. (1)–(4) and boundary conditions

Author's personal copy

Y. A. Kurdyaeva et al.   Pure Appl. Geophys.

listed at the end of Sect. 2.1 with analytical solution of the respective linearized equations.

In the case of an isothermal atmosphere (the background temperature T_0 of atmospheric gas is a constant), the background atmospheric gas density varies exponentially with height: $(T_0 = \text{const})$, $\rho_0(z) = \rho_{00} \exp(-z/H_0), H_0 = RT_0/(\mu g)$. In a comparison between analytical and numerical solutions, we take $H_0 = 8$ km and assume $\omega z = 0$, because the Coriolis effects on high-frequency AGWs are negligible. For the set of linearized Eq. (10) in isothermal background conditions, the following wave stationary solution can be obtained using standard methods described by Gossard and Hooke (1975) and Beer (1974):

$$u(x,z,t) = C \frac{gH_0 e^{\alpha z} k \cos(S)}{\omega}, \ S = kx + mz - \omega t,$$

$$R(x,z,t) = Ce^{\alpha z}\left[\left(\frac{gH_0 k^2}{\omega^2} + \frac{mA}{\omega}\right)\sin(S)\right.$$
$$\left. + \frac{\left(4m^2 H_0^2 B + 2A + B\right)}{4H_0 \omega}\cos(S)\right], \Theta(x,z,t)$$
$$= Ce^{\alpha z}\left[\left(1 - \frac{gH_0 k^2}{\omega^2} - \frac{mA}{\omega}\right)\sin(S)\right.$$
$$\left. - \frac{(4m^2 H_0 B + 2A + B)}{4H_0 \omega}\cos(S)\right], w(x,z,t)$$
$$= A(R + \Theta) + B\frac{\partial}{\partial z}(R + \Theta),$$

$$(18)$$

where k and m are the horizontal and vertical wave numbers, respectively; ω is the wave frequency; $\alpha = (2H_0)^{-1}$, A and B are coefficients having the forms of

$$A = \frac{\left(\gamma - 2\gamma m^2 H_0^2 - 2\right)\left(\gamma g H_0 k^2 - \omega^2\right)}{m\omega\left(4 - 4\gamma + \gamma^2 + 4\gamma^2 m^2 H_0^2\right)}, B$$
$$= \frac{2(2 - \gamma)\left(\gamma g H_0 k^2 - \omega^2\right)}{m\omega\left(4 - 4\gamma + \gamma^2 + 4\gamma^2 m^2 H_0^2\right)}$$

$$(19)$$

Wave numbers k, m and frequency ω are connected by the dispersion relation

$$\omega^2 = \frac{1}{2}\gamma g H_0\left(m^2 + k^2 + \alpha^2\right)$$
$$\left(1 \pm \sqrt{1 - \frac{4k^2(\gamma - 1)}{\gamma^2 H_0^2(m^2 + k^2 + \alpha^2)^2}}\right)$$

$$(20)$$

Here the signs $+$ and $-$ before the square root correspond to acoustic and internal gravity waves (IGWs), respectively. In Eqs. (18–20), an upward-directed group velocity corresponds to $m > 0$ for acoustic and $m < 0$ for internal gravity waves. Numerical simulations for comparisons with analytical solutions (18)–(20) are made with the AtmoSym (2016) model using the three-dimensional algorithms for solving Eqs. (1)–(4) developed by Gavrilov and Kshevetskii (2015). We use the initial conditions (11), conditions at the horizontal boundaries (6) and at the upper boundary (7). At the lower boundary $z = 0$, we use Neumann conditions (16) and specify the plane-wave pressure variation:

$$P(x, y, z = 0, t) = C \sin(kx - \omega t), \quad (21)$$

where C is the surface pressure amplitude. Relative density variations at the lower boundary are calculated using Eq. (17). Numerical results are obtained using the AtmoSym (2016) model for solving the equation set (1)–(4) with initial state (11) and conditions (6) at the horizontal boundaries, (7) at the upper boundary, also (16), (17), (21) at the lower boundary. In test runs, the atmosphere is isothermal with $H_0 = 8$ km. The wave forcing (21) with $C = 0.00001$, $k = 40\pi/L_x$, $L_x = 10^3$ km and frequencies $\omega = \pi/60 \ \text{s}^{-1}$ for the acoustic wave mode and $\omega = \pi/1800 \ \text{s}^{-1}$ for the IGW mode are activated at $t = 0$ s. The horizontal and vertical grid steps are 500 and 75 m, respectively, the time step is 0.14 s. Previous simulations with the model (e.g., Gavrilov and Kshevetskii 2015) showed the existence of a transition interval after initiating the boundary forcing at $t = 0$ s before the solution comes to a quasi-stationary regime. To diminish the initial AGW pulse, the surface wave source (21) was multiplied by factor $q = 1 - \exp(-t/t_0)$ with $t_0 = 2$ min. This factor gradually increases in time from 0 to 1 and the intensity of initial AGW pulse becomes smaller.

In the stationary regime, a good agreement between the numerical results and the analytical solution (18)–(20) in the free atmosphere, where AGW amplitudes and turbulent viscosity and heat conductivity are small, can be expected. Figure 2 shows numerical and analytical temperature and vertical velocity wave fields in the lower atmosphere at different t for the acoustic and IGW modes.
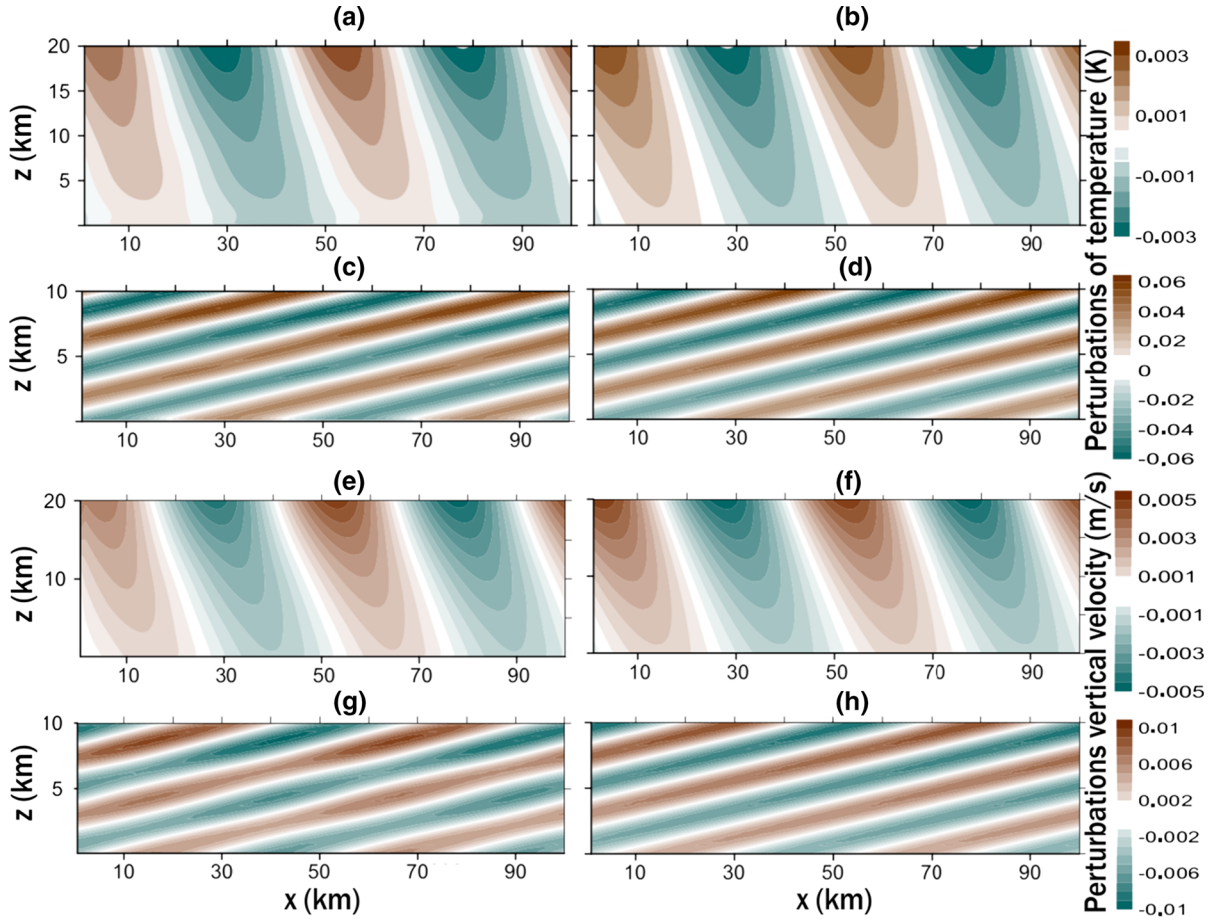
Figure 2
Perturbations of temperature (K) (**a–d**) and vertical velocity (m/s) (**e–h**) produced by the acoustic wave at $t \approx 16$ min (**a, b** and **e, f**) and by the internal gravity wave at $t \approx 4$ h (**c, d** and **g, h**) simulated numerically (left) and calculated using Eq. (18)–(20) according to the linear AGW theory (right)
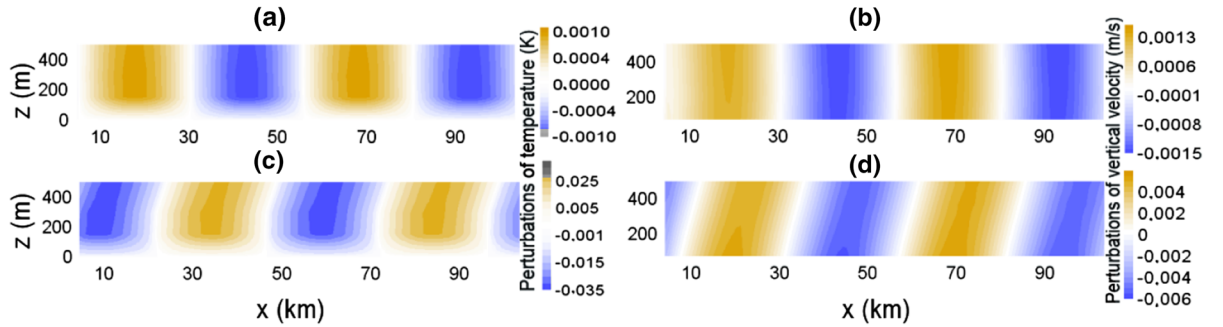

Figure 3
Simulated temperature (K) (left) and vertical velocity (m/s) (right) perturbations near the Earth's surface produced by the acoustic wave at $t \approx$ 16 min (**a, b**) and by the internal gravity wave at $t \approx 4$ h (**c, d**)

Similarities of the left and right panels outside the turbulized boundary layer in Fig. 2 show good agreement between nonlinear numerical and linear analytical solutions for small amplitude nondissipative AGWs.

In the boundary layer, increased turbulent dissipation and the lower boundary conditions (16) can produce differences between the numerical and analytical solutions (e.g., Gavrilov and Kshevetskii 2015). Figure 3 represents numerical solutions for temperature and vertical velocity with better vertical resolution near the lower boundary. One can see zero values of temperature perturbations the Earth's surface according to (16). However, at $z > 100$–150 m outside the boundary layer, the numerical solutions follow the analytical linear relations (18)–(20) for the free atmosphere. For vertical velocity, the Neumann lower boundary condition (16) gives even better agreement between the numerical and analytical solutions near the ground in the right plots of Fig. 3. This shows that the lower boundary conditions (13), (16) and (17) allow us selecting the AGW modes generated or reflected at the Earth's surface, which fits to the observed surface pressure and can propagate to the upper atmosphere.

5. Simulation for Observed Local Pressure Variations

To show capability of the numerical model for real data, we used a sample of the surface pressure
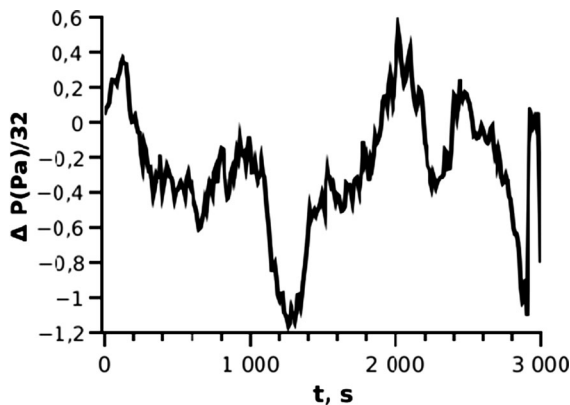

Figure 4
Surface pressure variations near Moscow on April 9, 2016

variations in time, $f(t)$, recorded with microbarograph at the Obukhov Institute of Atmospheric Physics near Moscow (55.7 N, 37.6 E) on April 9, 2016 as shown in Fig. 4. In Fig. 4, the factor 32 is due to the peculiarities of this particular microbarograph (the measurements are indirect, and the microbarograph digitizes the current in the instrument, but not the pressure, and the multiplier 32 is intended to recalculate the instrument's readings into pressure). The purpose of the simulations below is only to demonstrate the working capacity of the developed mathematical methods and the computer codes, and for such a demonstration it is sufficient to use the data of only one microbarograph. In Europe and in Africa there are nets of microbarographs, which in the future are supposed to be used to simulate waves from pressure variations on the Earth's surface. However, this net is not dense, and there is a question of how to fill in the missing data. This issue will be studied later, and accordingly, studies based on the data of the world net of microbarographs will be carried out at the next stage. Assuming a wave source near the measuring location (x_0, y_0), the lower boundary condition (13) for surface pressure is taken in the following form:

$$P(x, y, z = 0, t) = \exp[-((x - x_0)^2 + (y - y_0)^2)/d^2]f(t) \tag{22}$$

where d is the half-width of the wave source region. For present simulations we set $d = 2$ km. Other initial and boundary conditions are the same as in Sect. 2.2. The simulation starts from zero wave perturbations (11). Previous simulations with the AtmoSym (Gavrilov and Kshevetskii 2014a, 2015) showed an initial AGW pulse caused by the abrupt activation of wave source at $t = 0$. This pulse propagates upwards and in 15–20 min reaches altitudes 300–400 km, where initial AGWs dissipate due to high molecular viscosity and heat conduction. After the initial pulse dissipation, the results of numerical solution could be considered as upward propagating AGWs corresponding to measured variations of surface pressure shown in Fig. 4.

Simulated temperature fields for $t \approx 30$ min and $t \approx 45$ min after the wave source activation are shown in Fig. 5a, b, respectively. It can be seen that AGWs
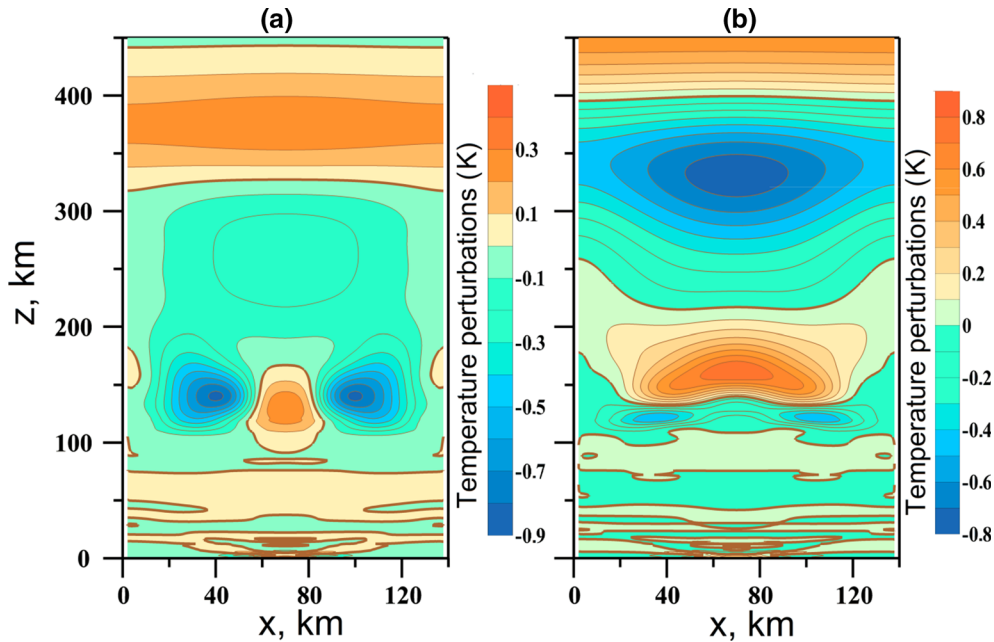
Figure 5
Simulated temperature perturbations (K) due to AGWs excited by the observed surface pressure variations as shown in Fig. 3 at $t = 30$ min (**a**) and $t = 45$ min (**b**). Thick lines correspond to zero contours

are propagating upwards with small amplitude increasing with height. These AGWs do not have large amplitudes because the pressure measurements of Fig. 5 correspond to quiet meteorological conditions near the observation site. In addition, observed variations of the surface pressure are relatively slow and generate mainly IGWs having the group velocity smaller than the sound speed and reaching the upper atmosphere later than the initial acoustic pulse (see Gavrilov and Kshevetskii 2014b). These IGWs produce wave fields as shown in Fig. 5a, b.

Localized wave source (22) may correspond to a region of local convection, which generates increased AGWs propagating downwards, reflected at the Earth's surface and going to the upper atmosphere. In the atmosphere, there are many sources of AGWs (meteorological fronts, wind shears, and orography) that propagate along the Earth's surface. Therefore, the pressure variations may be not localized in space and time. However, the wave source (22) gives simple approximation, which can be adjusted to many typical distributions of the surface pressure and it is

enough to demonstrate the AtmoSym simulating capacity and efficiency.

The preparation of more realistic boundary pressure field for the numerical simulations requires accurate assimilation of microbarograph pressure observations. This problem is out the scope of the present paper. Preparation of the boundary data for wide region requires measurements with a network of microbarographs.

The effects of nonlinearity of Eqs. (1)–(4) and AGW dissipation can substantially affect the wind velocity and temperature fields in the upper atmosphere at altitudes higher than 70 km. This paper is devoted to the technical problems of lower boundary conditions and we do not consider AGW effects on the upper atmosphere. However, there are previous publications devoted to the influence of waves on the mean wind velocity and temperature in the upper atmosphere (Gavrilov and Kshevetskii 2014b, 2015; Karpov and Kshevetskii 2014). These simulations were performed using some other wave sources, but they have demonstrated the AtmoSym capabilities for simulating the heating of the atmosphere and the

influence of waves on the mean wind in the upper atmosphere.

6. *Conclusion*

In this study, we set-up and mathematically investigated the problem of propagating nonlinear acoustic-gravity waves corresponding to the observed pressure variations, which are generated or reflected from the surface of the Earth. We also compared the results with analytical solutions of linear AGW theory.

Mathematical study showed that solutions of problem of AGW propagation from variable density and temperature specified on the Earth's surface are uniquely identified by the pressure on the Earth's surface, but do not depend on details of individual temperature and density distributions. Selection of upward propagating AGWs generated or reflected at the Earth's surface requires the Neumann conditions of the second kind involving vertical gradients of vertical velocity at the lower boundary. Numerically simulated AGW modes corresponding to harmonic variations of pressure at the Earth's surface confirmed the theoretical results.

The problem of waves propagating from a harmonic source specified at the lower boundary border can be solved analytically in the case of isothermal atmosphere. We compared analytical and numerical solutions and demonstrated good agreement between them. Such comparisons can be used for validating numerical models of atmospheric AGWs.

Reasonable agreement of wave parameters calculated using numerical simulation and analytical formulae can be considered as an indication of adequate description of wave processes by the nonlinear numerical model. An example is shown of numerical solution of AGW propagation from localized region of variations in the surface atmospheric pressure. Model of direct numerical simulation can be effective for simulating AGWs produced by variations of atmospheric pressure and for testing and validation of simplified parameterizations of wave effects in the atmosphere.

6.1. *Computer Code Availability*

The computer code is available for free online simulations for all users (see AtmoSym 2016). The code can be distributed and used with the permission from the Immanuel Kant Baltic Federal (the official owner of the code). Access to the fully functional demo-version of the AtmoSym computer code, which calculates the experiments described in the present paper, can be granted on demand by request to Sergej Kshevtskii (spkshev@gmail.com) or Yulia Kurdyaeva (yakurdyaeva@gmail.com). Any questions should be directed to the authors.

Acknowledgements

REFERENCES

Alexander, M., May, P., & Beres, J. (2004). Gravity waves generated by convection in the Darwin area during the Darwin Area Wave Experiment. *Journal of Geophysical Research, 109,* D20S04. (**1–11**).

Andreassen, O., Hvidsten, O., Fritts, D., & Arendt, S. (1998). Vorticity dynamics in a breaking internal gravity wave, Part 1 Initial instability evolution. *Journal of Fluid Mechanics, 367,* 27–46.

AtmoSym: A multi-scale atmosphere model from the Earth's surface up to 500 km. http://atmos.kantiana.ru. 2016. Accessed 10 Apr 2017.

Babkovskaia, N., Haugen, N., & Brandenburg, A. (2011). A high-order public domain code for direct numerical simulations of turbulent combustion. *Journal of Computational Physics, 230,* 1–12.

Baker, D., & Schubert, G. (2000). Convectively generated internal gravity waves in the lower atmosphere of Venus, Part II mean

wind shear and wave–mean flow interaction. *Journal of the Atmospheric Sciences, 57,* 200–215.

Balachandran, N. K. (1980). Gravity waves from thunderstorms. *Monthly Weather Review, 108,* 804–816.

Banks, P. M., & Kockarts, G. (1973). *Aeronomy, Part B*. New York: Elsevier.

Beer, T. (1974). *Atmospheric waves*. London: Adam Hilder.

Blanc, E., Farges, T., Le Pichon, A., & Heinrich, P. (2014). Ten year observations of gravity waves from thunderstorms in western Africa. *Journal of Geophysical Research: Atmospheres, 119,* 6409–6418. https://doi.org/10.1002/2013JD020499.

Brekhovskikh, L., & Godin, O. (1990). *Acoustics of layered media*. Berlin: Springer.

Courant, R., & Hilbert, D. (1962). *Methods of mathematical physics. 2. Partial differential equations*. Singapore: Wiley-VCH GmbH & Co.

Dalin, P., Gavrilov, N., Pertsev, N., Perminov, V., Pogoreltsev, A., Shevchuk, N., et al. (2016). A case study of long gravity wave crests in noctilucent clouds and their origin in the upper tropospheric jet stream. *Journal of Geophysical Research: Atmospheres, 121,* 1402–14116. https://doi.org/10.1002/2016jd025422.

Fovell, R., Durran, D., & Holton, J. R. (1992a). Numerical simulation of convectively generated stratospheric gravity waves. *Journal of the Atmospheric Sciences, 47,* 1042.

Fovell, R., Durran, D., & Holton, J. R. (1992b). Numerical simulation of convectively generated stratospheric gravity waves. *Journal of the Atmospheric Sciences, 47,* 1427–1442.

Fritts, D. C., & Alexander, M. J. (2003). Gravity wave dynamics and effects in the middle atmosphere. *Reviews of Geophysics, 41,* 1003. https://doi.org/10.1029/2001RG000106.

Fritts, D. C., & Garten, J. F. (1996). Wave breaking and transition to turbulence in stratified shear flows. *Journal of the Atmospheric Sciences, 53,* 1057–1085.

Fritts, D. C., Vadas, S. L., Wan, K., & Werne, J. A. (2006). Mean and variable forcing of the middle atmosphere by gravity waves. *Journal of Atmospheric and Solar-Terrestrial Physics, 68,* 247–265.

Gavrilov, N. M. (2013). Estimates of turbulent diffusivities and energy dissipation rates from satellite measurements of spectra of stratospheric refractivity perturbations. *Atmospheric Chemistry and Physics, 13,* 12107–12116. https://doi.org/10.5194/acp-13-12107-2013.

Gavrilov, N. M. & Fukao, S. (1999). A comparison of seasonal variations of gravity wave intensity observed by the MU radar with a theoretical model. *Journal of the Atmospheric Sciences, 56,* 3485–3494. https://doi.org/10.1175/1520-0469(1999)056<3485:acosvo>2.0.co;2.

Gavrilov, N. M., & Kshevetskii, S. P. (2013). Numerical modeling of propagation of breaking nonlinear acoustic-gravity waves from the lower to the upper atmosphere. *Advances in Space Research, 51,* 1168–1174. https://doi.org/10.1016/j.asr.2012.10.023.

Gavrilov, N. M., & Kshevetskii, S. P. (2014a). Numerical modeling of the propagation of nonlinear acoustic-gravity waves in the middle and upper atmosphere. *Izvestiya, Atmospheric and Oceanic Physics, 50,* 66–72. https://doi.org/10.1134/S0001433813050046.

Gavrilov, N. M., & Kshevetskii, S. P. (2014b). Three-dimensional numerical simulation of nonlinear acoustic-gravity wave propagation from the troposphere to the thermosphere. *Earth Planets Space, 66,* 88. https://doi.org/10.1186/1880-5981-66-88.

Gavrilov, N. M., & Kshevetskii, S. P. (2015). Dynamical and thermal effects of nonsteady nonlinear acoustic-gravity waves propagating from tropospheric sources to the upper atmosphere. *Advances in Space Research*. https://doi.org/10.1016/j.asr.2015.01.033.

Gavrilov, N. M., & Yudin, V. A. (1992). Model for coefficients of turbulence and effective Prandtl number produced by breaking gravity waves in the upper atmosphere. *Journal of Geophysical Research, 97,* 7619–7624. https://doi.org/10.1029/92jd00185.

Gossard, E. E., & Hooke, W. H. (1975). *Waves in the atmosphere*. Amsterdam: Elsevier.

Janjic, Z. I. (2002). A nonhydrostatic model based on new approach. *Meteorology and Atmospheric Physics, 82*(1), 271–285.

Janjic, Z. I. (2006). The WRF NMM core. Overview of basic principles (presented by T. Black). NCEP. http://www.dtcenter.org/wrf-nmm/users/docs. Accessed 10 Jun 2017.

Jonson, R. H., & Young, G. S. (1983). Heat and moisture budgets of tropical mesoscale anvil clouds. *Journal of the Atmospheric Sciences, 80,* 2138–2147.

Karpov, I. V., & Kshevetskii, S. P. (2014). Formation of large-scale disturbances in the upper atmosphere caused by acoustic-gravity wave sources on the Earth's surface. *Geomagnetism and Aeronomy, 54*(4), 553–562. https://doi.org/10.1134/S0016793214040173.

Khairoutdinov, M. F., Krueger, S. K., Moeng, C.-H., Bogenschutz, P. A., & Randall, D. A. (2009). Large-eddy simulation of maritime deep tropical convection. *Journal of Advances in Modeling Earth Systems, 1*(15), 13.

Kherani, E. A., Lognonne, P., Hebert, H., Rolland, L., Astafyeva, E., Occhipinti, G., et al. (2012). Modelling of the total electronic content and magnetic field anomalies generated by the 2011 Tohoku-Oki tsunami and associated acoustic-gravity waves. *Geophysical Journal International, 191,* 1049–1066. https://doi.org/10.1111/j.1365-246X.2012.05617.x.

Kshevetskii, S. P. (2001). Modelling of propagation of internal gravity waves in gases. *Computational Mathematics and Mathematical Physics, 41,* 295–310.

Kshevetskii, S. P. (2002). Internal gravity waves in non-exponentially density-stratified fluids. *Computational Mathematics and Mathematical Physics, 42*(10), 1510–1521.

Kshevetskii, S. P., & Kulichkov, S. N. (2015). Effects that internal gravity waves from convective clouds have on atmospheric pressure and spatial temperature-disturbance distribution. *Atmospheric and Oceanic Physics, 51*(1), 42–48. https://doi.org/10.1134/S0001433815010065.

Lax, P. D. (1957). Hyperbolic systems of conservation laws. *Communications on Pure and Applied Mathematics, 10,* 537–566.

Lax, P. D., & Wendroff, B. (1960). Hyperbolic systems of conservation laws. *Communications on Pure and Applied Mathematics, 13,* 217–237.

Leble, S., & Perelomova, A. (2013). Problem of proper decomposition and initialization of acoustic and entropy modes in a gas affected by the mass force. *Applied Mathematical Modelling, 37,* 629–635.

Liu, H.-L., Foster, B. T., Hagan, M. E., McInerney, J. M., Maute, A., Qian, L., et al. (2010). Thermosphere extension of the whole

atmosphere community climate model. *Journal of Geophysical Research, 115,* A12302. https://doi.org/10.1029/2010JA015586.

Liu, X., Xu, J., Liu, H.-L., & Ma, R. (2008). Nonlinear interactions between gravity waves with different wavelengths and diurnal tide. *Journal of Geophysical Research, 113,* D08112. https://doi.org/10.1029/2007JD009136.

Matsumura, M., Saito, A., Iyemori, T., Shinagawa, H., Tsugawa, T., Otsuka, Y., Nishioka, M., & Chen, C. H. (2011). Numerical simulations of atmospheric waves excited by the 2011 off the Pacific coast of Tohoku Earthquake. *Earth, Planets and Space 63*(7), 885–889.

Medvedev, A. S., & Gavrilov, N. M. (1995). The nonlinear mechanism of gravity wave generation by meteorological motions in the atmosphere. *Journal of Atmospheric and Terrestrial Physics, 57,* 1221–1231.

Miller, D. V. (1999). Thunderstorm induced gravity waves as a potential hazard to commercial aircraft. *American Meteorological Society 79th Annual conference*, Windham Anatole Hotel, Dallas, TX, January 10–15. Dallas: American Meteorological Society.

Pedloski, J. (2006). *Geophysical fluid dynamics*. Berlin: Springer.

Picone, J. M., Hedin, A. E., Drob, D. P., & Aikin, A. C. (2002). NRL-MSISE-00 empirical model of the atmosphere: statistical comparisons and scientific issues. *Journal of Geophysical Research*. https://doi.org/10.1029/2002JA009430.

Pielke, R. A., Cotton, W. R., Walko, L. R., Tremback, C. J., Lyons, W. A., Grasso, L. D., et al. (1992). A comprehensive meteorological modeling system—RAMS. *Meteorology and Atmospheric Physics, 49*(1–4), 69–91.

Pierce, A. D., & Coroniti, S. C. (1966). A mechanism for the generation of acoustic-gravity waves during thunder-storm formation. *Nature, 210,* 1209–1210. https://doi.org/10.1038/2101209a0.

Plougonven, R., & Snyder, Ch. (2007). Inertia-gravity waves spontaneously generated by jets and fronts. Part I: Different baroclinic life cycles. *Journal of the Atmospheric Sciences, 64,* 2502–2520.

Plougonven, R., & Zhang, F. (2014). Internal gravity waves from atmospheric jets and fronts. *Reviews of Geophysics*. https://doi.org/10.1002/2012RG000419.

Sao Sabbas, F. T., Rampinelli, V. T., & Santiago, J. (2009). Characteristics of sprite and gravity wave convective sources present in satellite IR images during the SpreadFEx 2005 in Brazil. *Annales Geophysics, 27,* 1279–1293.

Shinagawa, H., Iyemori, T., Saito, S., & Maruyama, T. (2007). A numerical simulation of ionospheric and atmospheric variations associated with the Sumatra earthquake on December 26, 2004. *Earth Planets Space, 59,* 1015–1026.

Snively, J. B., & Pasko, V. B. (2003). Breaking of thunderstorm generated gravity waves as a source of short period ducted waves at mesopause altitudes. *Geophysical Research Letters, 30*(24), 2254. https://doi.org/10.1029/2003GL018436.

Yu, Y., Hickey, M. P., & Liu, Y. (2009). A numerical model characterizing internal gravity wave propagation into the upper atmosphere. *Advances in Space Research, 44,* 836–846. https://doi.org/10.1016/j.asr.2009.05.014.